View metadata, citation and similar papers at core.ac.uk
brought to you by CORE
provided by Columbia University Academic Comm

JOURNAL OF GEOPHYSICAL RESEARCH, VOL. 117, D19106, doi:10.1029/2012JD017777, 2012

Why might stratospheric sudden warmings occur with similar frequency in El Niño and La Niña winters?

C. I. Garfinkel,[1] A. H. Butler,[2] D. W. Waugh,[1] M. M. Hurwitz,[3,4] and L. M. Polvani[5,6]

Received 13 March 2012; revised 3 August 2012; accepted 17 August 2012; published 4 October 2012.

[1] The effect of El Niño-Southern Oscillation (ENSO) on the frequency and character of Northern Hemisphere major mid-winter stratospheric sudden warmings (SSWs) is evaluated using a meteorological reanalysis data set and comprehensive chemistry-climate models. There is an apparent inconsistency between the impact of opposite phases of ENSO on the seasonal mean vortex and on SSWs: El Niño leads to an anomalously warm, and La Niña leads to an anomalously cool, seasonal mean polar stratospheric state, but both phases of ENSO lead to an increased SSW frequency. A resolution to this apparent paradox is here proposed: the region in the North Pacific most strongly associated with precursors of SSWs is not strongly influenced by El Niño and La Niña teleconnections. In the observational record, both La Niña and El Niño lead to similar anomalies in the region associated with precursors of SSWs and, consistent with this, there is a similar SSW frequency in La Niña and El Niño winters. A similar correspondence between the penetration of ENSO teleconnections into the SSW precursor region and SSW frequency is found in the comprehensive chemistry-climate models. The inability of some of the models to capture the observed relationship between La Niña and SSW frequency appears related to whether the modeled ENSO teleconnections result in extreme anomalies in the region most closely associated with SSWs. Finally, it is confirmed that the seasonal mean polar vortex response to ENSO is only weakly related to the relative frequency of SSWs during El Niño and La Niña.

Citation: Garfinkel, C. I., A. H. Butler, D. W. Waugh, M. M. Hurwitz, and L. M. Polvani (2012), Why might stratospheric sudden warmings occur with similar frequency in El Niño and La Niña winters?, *J. Geophys. Res.*, *117*, D19106, doi:10.1029/2012JD017777.

1. Introduction

[2] The El Niño - Southern Oscillation (ENSO) is the dominant mode of interannual variability in the Tropics, and it has well-known teleconnections with the Northern Hemisphere (NH) midlatitudes [*Horel and Wallace*, 1981]. During an El Niño winter (hereafter EN), mid-tropospheric geopotential heights are anomalously low in the North Pacific, and vice versa for La Niña winters (hereafter LN) (e.g., Figures 1a for EN and 1b for LN). Recently, these teleconnections with the midlatitudes have been shown to influence the wintertime NH stratospheric polar vortex [*Manzini et al.*, 2006; *Garfinkel and Hartmann*, 2008; *Ineson and Scaife*, 2009; *Bell et al.*, 2009]. During LN, opposite-signed, but weaker, seasonal-mean stratospheric anomalies appear to be present in both observations and models forced with observed sea surface temperatures [*Sassi et al.*, 2004; *Manzini et al.*, 2006; *Garfinkel and Hartmann*, 2007; *Brönnimann*, 2007; *Free and Seidel*, 2009; *Mitchell et al.*, 2011].

[3] Occasionally, the polar vortex completely breaks down, whereby zonal winds change from strong, climatological (>40m/s) westerlies to easterlies at 10 hPa, 60°N. Such events are known as major stratospheric sudden warmings (SSWs), and are preceded by a burst of wave activity from the troposphere into the stratosphere [*Matsuno*, 1971]. *Nishii et al.* [2009] and *Garfinkel et al.* [2010] show that on intraseasonal timescales, low height anomalies in the North Pacific can lead to such a burst of wave activity. Because a trough of the climatological planetary wave pattern (and of both wave number 1 and wave number 2 separately) is located in the North Pacific, an anomalous low in the North Pacific will enhance the climatological planetary waves in the troposphere.

[1]Department of Earth and Planetary Science, Johns Hopkins University, Baltimore, Maryland, USA.
[2]Climate Prediction Center, NCEP, NOAA, Camp Springs, Maryland, USA.
[3]Goddard Earth Sciences Technology and Research, Morgan State University, Baltimore, Maryland, USA.
[4]NASA Goddard Space Flight Center, Greenbelt, Maryland, USA.
[5]Department of Applied Physics and Applied Mathematics and Department of Earth and Environmental Sciences, Columbia University, New York, New York, USA.
[6]Lamont-Doherty Earth Observatory, Columbia University, Palisades, New York, USA.

Corresponding author: C. I. Garfinkel, Department of Earth and Planetary Science, Johns Hopkins University, Baltimore, MD 21209, USA. (cig4@jhu.edu)

©2012. American Geophysical Union. All Rights Reserved.
0148-0227/12/2012JD017777

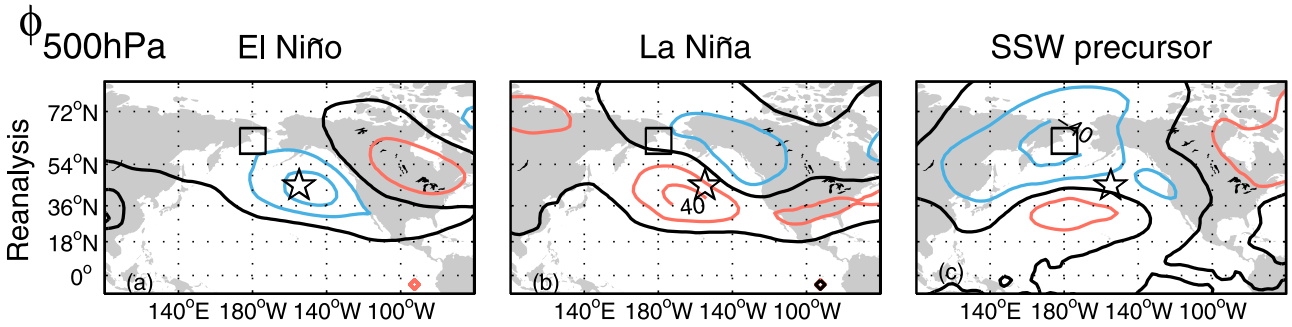

Figure 1. Geopotential height anomalies at 500 hPa in NDJFM, in the ECMWF reanalysis data during (a) a composite of El Niño and (b) La Niña events, and (c) 5–20 days preceding major sudden stratospheric warmings. The contour interval is 10 m. Squares and stars are included in each plot at 62.5°N, 180°E and 45°N, 205°E; see the text for details. The zero line is shown in black.

Once the resulting stronger planetary wave propagates upwards and breaks in the stratosphere, it will weaken the polar vortex. In contrast, an anomalous ridge in this region leads to an intensification of the vortex [*Limpasuvan et al.*, 2005; *Woollings et al.*, 2010; *Nishii et al.*, 2010]. Once a SSW occurs, it can influence jets in the troposphere in the weeks or months following an event [*Polvani and Waugh*, 2004; *Limpasuvan et al.*, 2004] and thereby impact surface climate. A better understanding of the connection between ENSO and SSWs might therefore lead to improved tropospheric seasonal forecasts for ENSO winters and understanding of Arctic ozone variability [*Baldwin et al.*, 2003; *Cagnazzo et al.*, 2009].

[4] *Butler and Polvani* [2011] (hereafter BP11) recently revisited the ENSO-stratosphere connection and found that from 1958 to 2010, SSWs occur just as often during EN winters as during LN winters, contrary to the modeling study of *Taguchi and Hartmann* [2006]. BP11 also found that major SSWs occur nearly twice as often during both EN and LN winters as compared to ENSO-neutral winters. Even though EN and LN lead to opposite signed seasonal mean vortex anomalies, they both lead to more SSWs. Figure 2 displays this graphically: even though the mean state differs between EN and LN winters, the extremes are indistinct. In contrast, the mean states of ENSO active years (i.e., either EN or LN) and ENSO neutral years are indistinguishable, but the vortex is more variable during ENSO active years. Finally, the SSW frequencies during each ENSO phase are consistent with the heat flux anomalies in the lower stratosphere: even though the seasonal mean distribution of zonal wave number-1 and −2 heat flux differs between EN and LN (Figures 3a and 3b, as in *Taguchi and Hartmann* [2006] and *Garfinkel and Hartmann* [2008]), the frequency of large positive heat flux anomalies is greater during LN winters than during neutral ENSO winter (or even during EN winters).

[5] In this paper, we investigate how (and why) LN and EN can both lead to increased SSW frequency, and, at the same time, to opposite signed seasonal mean vortex anomalies. We also consider whether comprehensive chemistry-climate models (CCMs) can capture this effect. Section 2 will introduce the data sources and the methods used. Section 3.1 will

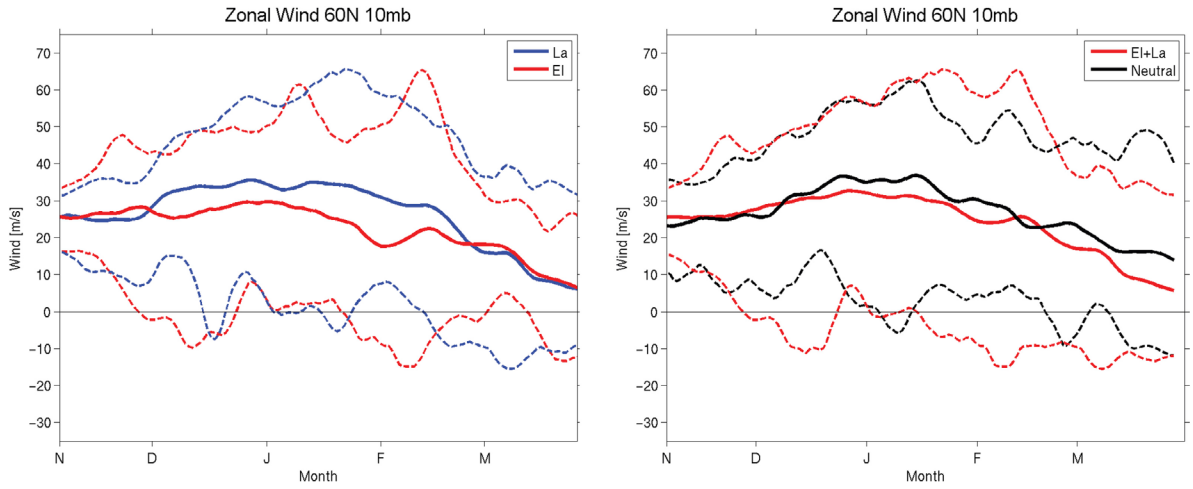

Figure 2. Zonal wind at 60N, 10 hPa in the reanalysis data during (left) a composite of El Niño and La Niña events, and (right) ENSO active and neutral ENSO events. Bold lines show the mean wind, and dashed lines show the largest extreme. A 7-point running mean filter has been applied in order to smooth the data. The years selected for each composite can be found in Table 1 and are chosen with the 0.5C threshold.

show that the tropospheric teleconnections associated with ENSO are consistent with an increased SSW frequency (hereafter, fSSW) in both EN and LN winters in the observational record. We will then test the explanation offered in Section 3.1 by examining fSSW in CCMs in Section 3.2, where we will show that fSSW during EN and LN winters in CCMs is also related to whether ENSO teleconnections result in extreme anomalies in the region most closely associated with SSWs. In contrast, the seasonal mean stratospheric response to ENSO is very weakly related to LN and EN SSW frequency. Section 3.3 will show that models that do not capture some of the subtle details of LN teleconnections and SSWs also fail to capture an enhanced fSSW in LN. The appendix will discuss the preconditioning of the vortex, the strength of the SSWs, and the morphology of the SSWs, for the SSWs during EN and LN.

2. Data and Methods

2.1. Data

[6] We evaluate the connection between ENSO and SSWs in both the ECMWF reanalysis record (ERA40 [*Uppala et al.*, 2005] through 2002 and 2 additional years of operational data) and integrations of a range of CCMs. The first group of models evaluated are the "REF-B1" simulations as defined by the Chemistry-Climate Model Validation project phase 2 (CCMVal-2) project [*SPARC CCMVal*, 2010; *Eyring et al.*, 2008] and provided to the CCMVal-2 database. The REF-B1 simulations are driven by annually varying emissions of ozone precursors, concentrations of ozone-depleting substances and greenhouse gases, sea surface temperatures (SSTs), and sea ice. We examine the Canadian Middle-Atmosphere Model (CMAM [*Scinocca et al.*, 2008]), Goddard Earth Observing System CCM, Version 2 (GEOSCCM [*Rienecker et al.*, 2008; *Hurwitz et al.*, 2010, section 2]), UMSLIMCAT [*Tian and Chipperfield*, 2005], CCSRNIES [*Akiyoshi et al.*, 2009], and UMUKCA-METO [*Morgenstern et al.*, 2009]. These models are chosen because daily gridded geopotential height in the troposphere is available and fSSW is at least 3 events per decade (as compared to ~6 in the observational record).

[7] One additional model, LMDZrepro3, meets this criteria, but we do not include it for the following reason. Preliminary work suggests that LMDZrepro3 has too many splitting type SSWs as opposed to displacement type SSWs [cf. *Charlton and Polvani*, 2007]. The tropospheric precursors of SSWs in this model are qualitatively different from those in other models and in the reanalysis record (not shown here, but they resemble wave number 2; see Figures 3b and 3d of *Garfinkel et al.* [2010] for an example). Additional work is planned to more fully understand the ability of this model (and other models in the CCMVal-2 archive) to capture the morphology of SSWs.

[8] In addition, we evaluate three 50-year-long GEOSCCM integrations in which all boundary conditions are identical except for the SST and sea ice climatologies, which correspond to perpetual EN, LN and neutral ENSO respectively. These long integrations are used to demonstrate the robustness of our results because every winter is in the same ENSO phase. In the EN experiment, the SSTs of July 1982–June 1983, July 1987–June 1988, and July 1997–June 1998 are composited together and used to drive the model with a repeating annual cycle. In the LN experiment, the SSTs of July 1988–June 1989 and July 1999–June 2000 are composited together and used to drive the model with a repeating annual cycle. The ENSO neutral experiment, as well as additional details of the model integration, are fully described in *Hurwitz et al.* [2011]. While the model parameterizations for the perpetual GEOSCCM integrations are not identical to those used in the experiment conducted for CCMVal-2 (e.g., the perpetual ENSO experiments include a new gravity wave drag scheme in which a QBO is internally generated, whereas the CCMVal-2 run does not include a QBO), the mean state and the variability of the NH stratosphere is well-reproduced in both. It is likely that differences between the two sets of results are due to differences in the experimental design rather than differences between the two model configurations. Specifically, the perpetual ENSO integrations are driven by SST anomalies from a small number of extreme events, while the CCMVal-2 integration is driven by observed SST from a range of ENSO events. Finally, we have examined the strength of the correlation between tropospheric variability and weakening of the vortex (i.e., Figure 1 of *Garfinkel et al.* [2010]), and GEOSCCM, unlike WACCM, accurately simulates the magnitude of the correlation. *SPARC CCMVal* [2010, p. 140] grades highly the representation of the Northern Hemisphere stratosphere by the GEOSCCM as compared to the multimodel mean.

2.2. Methods

[9] For the reanalysis and the CCMVal-2 model integrations, winters in which the November through March mean Niño3.4 index (available at http://www.cpc.ncep.noaa.gov/data/indices/ersst3b.nino.mth.ascii) exceeds 0.5°C are classified as an EN or LN event when calculating SSW frequency; see BP11 or Table 1 for a list of winters included. Results are robust to using the NDJ seasonal mean (rather than NDJFM) and to increasing the Nino 3.4 threshold to 0.75° or 1° (rather than 0.5°C). When we calculate ENSO teleconnections, we use a Niño3.4 threshold of 1C to show the effect of ENSO in the North Pacific more clearly. Six LN events and eight EN events exceeded this threshold; see Table 1 for a list. Results are robust to using the 0.5°C threshold. The "REF-B1" simulations covered the period 1960 to 2004; since we wish to include the same ENSO events for both the models and the reanalysis, we neglect the SSWs that have occurred in the observational record before 1960 or after 2004. Including these SSWs does not qualitatively affect our results.

[10] Anomalies are computed as follows. For the reanalysis and the CCMVal-2 model integrations, a daily climatology from 1960–2004 is formed and then subtracted from the raw fields to generate daily anomalies. For the reanalysis and models with leap years, June 20 of leap years is neglected. Results are identical if we smooth the daily climatology or if we subtract the 4 highest harmonics of the annual cycle to form anomalies. For the GEOSCCM perpetual ENSO experiments, a daily climatology of the ENSO neutral integration is formed and subtracted from the LN and EN integrations to generate daily anomalies. The seasonal mean polar vortex strength is defined as the 10 hPa, NDJFM, 70N and poleward area weighted average of the daily anomalies of geopotential height. Other wintertime

Table 1. Frequency (Freq) of SSW for the Observations (1960–2004 Only), the Perpetual ENSO GEOSCCM Integrations, and the CCMVal Integrations[a]

	SSW Frequency in Each Data Source											
	EN			LN			Neutral			All		
	Winters	SSW	Freq	Winters	SSW	Freq	Winters	SSW	Freq	Winters	SSW	Freq
Reanalysis	14	10	0.71	15	11	0.73	15	5	0.33	44	26	0.59
GEOSCCM perp. ENSO	50	35	0.70	50	9	0.18	50	16	0.32	150	60	0.40
GEOSCCM	14	11	0.79	15	7	0.47	15	8	0.53	44	26	0.59
UMSLIMCAT	14	13	0.93	15	12	0.80	15	9	0.60	44	34	0.77
CMAM, Ens. mean	42	41	0.98	45	46	1.02	45	40	0.89	132	127	0.96
UMUKCA-METO	14	13	0.93	15	6	0.40	15	9	0.60	44	28	0.64
CCSRNIES, Ens. mean	42	21	0.50	45	13	0.29	45	13	0.29	132	47	0.36

[a]The El Niño winters are 1963/64, 1965/66, 1968/ 69, 1969/70, 1972/73, 1976/77, 1977/78, 1982/83, 1986/87, 1987/88, 1991/92, 1994/95, 1997/98, and 2002/03. The 15 La Niña winters are 1962/63, 1964/65, 1967/68, 1970/71, 1971/72, 1973/74, 1974/75, 1975/76, 1983/84, 1984/85, 1988/89, 1995/96, 1998/99, 1999/2000, and 2000/01. The remaining winters are classified as ENSO neutral. The 8 El Niño winters in which Niño3.4 exceeds 1°C are 1965/66, 1972/73, 1982/83, 1986/87, 1991/92, 1994/95, 1997/98, and 2002/03. The 6 La Niña winters in which Niño3.4 is less than −1°C are 1970/71, 1973/74, 1975/76, 1988/89, 1998/99, and 1999/2000.

seasonal mean quantities are computed by averaging the daily anomalies during each NDJFM period.

[11] Three markers are placed on Figures 1, 6, and 7 to indicate important locations to which we refer throughout the paper. The 500 hPa height anomalies 5 to 20 days preceding SSWs in the reanalysis are composited together, and the center of the 20° latitude by 30° longitude region with the largest anomaly is indicated by a square. The square is located at 62.5°N, 180°E (i.e. the box extends from 52.5°N–72.5°N, 165°E–195°E) and this location is marked with a square on all of the panels. This region is referred to as the *SSW precursor region.* A similar procedure is followed for each CCM, and a diamond is used to indicate the center of the SSW precursor region for each CCM. While some previous authors have separated the tropospheric precursors associated with split or displacement type SSWs [e.g., *Cohen and Jones*, 2011], we do not for two reasons. First, the North Pacific is important for both wave-1 and wave-2 wave driving of the vortex and for both split and displacement type SSWs [*Garfinkel et al.*, 2010; *Cohen and Jones*, 2011]. Second, there is no strong preference for either type of SSW during either LN or EN (see the appendix for more details). Finally, the SSW precursor region in NASA's Modern-Era Retrospective Analysis for Research and Applications (MERRA) [*Rienecker et al.*, 2011] reanalysis is nearly identical [*Garfinkel et al.*, 2012].

[12] The star is used to indicate the center of the 20° latitude by 30° longitude region in which the difference between EN and LN height anomalies is maximized in the reanalysis record (i.e. 45°N, 205°E, the center of 35°N–55°N, 190°E–220°E). This location is referred to as *Gulf of Alaska center of ENSO teleconnections.* Results are robust to alteration of the size of the boxes. The location of the square and the star are the same in all figures, but the location of the diamond changes with each data source. Section 3 will discuss the relative ability of different phases of ENSO to influence anomalies in these regions.

3. ENSO and Tropospheric Precursors to SSWs

3.1. Observations

[13] In this section we develop an explanation for the similar fSSW in EN and LN winters in the observational record. We will then test this explanation in Section 3.2. Figures 1a and 1b show the teleconnections associated with LN and EN, and Figure 1c shows geopotential height anomalies at 500 hPa preceding SSWs (independent of ENSO phase). Prior to SSWs, a deep subpolar low height anomaly is centered just west of the dateline (denoted by a square on Figure 1). As discussed in the introduction, anomalously deep lows in this region constructively interfere with the stationary waves and weaken the vortex [*Garfinkel and Hartmann*, 2008; *Ineson and Scaife*, 2009; *Nishii et al.*, 2009; *Garfinkel et al.*, 2010]. Regardless of ENSO phase, low height anomalies in the North Pacific are present throughout the period in which the vortex is weakening (not shown). The key point of Figure 1 is that the anomalies preceding SSWs are different from the LN and EN teleconnections; namely, the anomalous low that precedes SSWs (the square) is to the northwest of the region where ENSO teleconnections are strongest (the star).

[14] While the teleconnections of EN and LN are to first order linear (i.e. equal in magnitude and opposite in sign), important deviations from linearity exist in the Northwest Pacific. Most importantly for SSWs, the anomalous low associated with EN extends into the subpolar Northwest Pacific where low anomalies can constructively interfere with the climatological planetary waves and thus increase planetary wave driving of the stratosphere. In contrast, the anomalous ridge associated with LN does not reach this region. The pattern correlation in the region 40N–75N, 165E–215E between LN's teleconnections and the anomalies preceding SSWs is 0.01. The difference between EN and LN teleconnections is significant only closer to the Gulf of Alaska. (We note, in passing, that our LN composite pattern differs in its details from that in *Hoerling et al.* [1997]. This difference could be due to the modern reanalysis product used here or due to the winter seasons chosen- 4 of the 9 LN winters in *Hoerling et al.* [1997] predate 1960 and are therefore outside of our analysis period.)

[15] It is conceivable that SSWs are caused mainly by extreme height anomalies, as linear quasi-geostrophic Eliassen Palm flux is related to the square of wave amplitude [*Dunkerton et al.*, 1981; *Andrews et al.*, 1987, pp. 188 and 231]. We therefore compute the probability of extreme negative height anomalies in the SSW precursor region

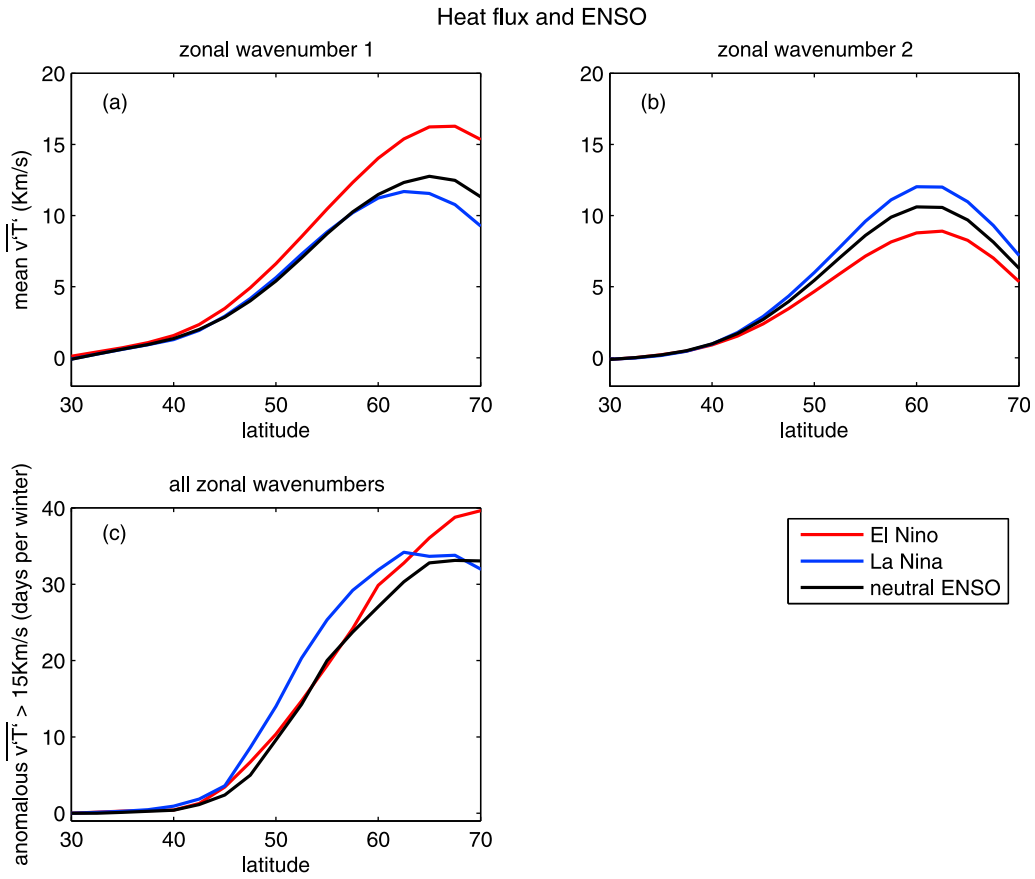

Figure 3. Heat flux ($\overline{v'T'}$) during EN, LN, and neutral ENSO at 70 hPa. (a) Seasonal mean (November–March) for zonal wave number 1, (b) like Figure 3a but for zonal wave number 2. (c) Number of days per winter in which heat flux anomalies exceed 15Km/s. Anomalies are computed as in section 2, and results are robust to changing the threshold to e.g., 10Km/s or 20Km/s. The years selected for each composite can be found in Table 1 and are chosen with the 0.5C threshold.

during EN winters, LN winters, and neutral ENSO winters. The percentage of winter days in which height anomalies in the SSW precursor region (i.e. surrounding the square on Figure 1) exceed −120 m is evaluated. Perhaps surprisingly, extreme negative anomalies occur most often during LN winters, and more often during EN winters than neutral ENSO winters, consistent with the respective SSW frequencies. The next section (and in particular Figures 5a, 5d, and 5e) will discuss this effect more quantitatively, but e.g., the increase during LN as compared to neutral ENSO is ∼20%. (Results are not sensitive to the threshold for classifying an extreme height anomaly.)

[16] A similar procedure can be followed for extreme height anomalies in the Gulf of Alaska in the region where ENSO teleconnections peak (denoted with a star on Figure 1). ENSO influences extreme height anomalies in the Gulf of Alaska; extreme negative anomalies occur in this region most often during EN and least often during LN (specifically, the frequency during EN is more than double that of LN, and this difference is significant at the 95% level by a Monte Carlo test in which winters are randomly characterized as EN or LN). However, the Gulf of Alaska is at the node of the pattern associated with tropospheric precursors of SSWs shown in Figure 1c. In contrast, LN is associated with a slight increase in frequency of extreme negative events in the SSW precursor region, consistent with the enhanced fSSW during LN. In the next section we will show that the LN to EN ratio of extreme height anomalies in the SSW precursor region is closely associated with the LN to EN ratio of fSSW in models as well.

3.2. Models

[17] We now discuss the fSSW during ENSO in a number of model integrations. Table 1 lists fSSW for each model considered, and these results are presented visually in Figure 4. While some models accurately capture the observed fSSW during the different ENSO phases (e.g., UMSLIMCAT), others do not (e.g., GEOSCCM and UMUKCA-METO). Using a Monte Carlo test to count SSWs in 10,000 random winters equal to the length of the GEOSCCM perpetual ENSO integrations (i.e. 50 years), the probability of a decrease in fSSW during LN relative to the other two integrations is found to be $p < 0.001$. Hence, some physical mechanism is almost certainly responsible for the reduced fSSW during LN in this model. An additional question we will address is: what might cause the inter-model variability in EN and LN SSW frequency?

[18] In Figure 5, we consider the relationship between LN and EN fSSW and the tropospheric teleconnections of ENSO for the models in Table 1 and thereby test the

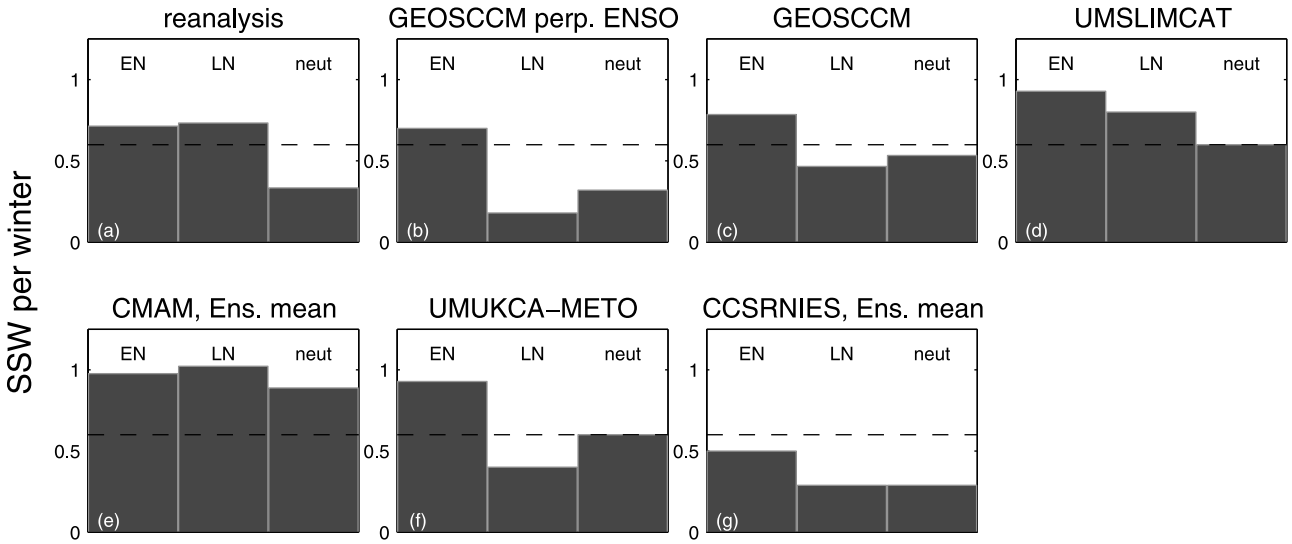

Figure 4. The frequency of sudden stratospheric warming events during La Niña, El Nino, and neutral ENSO winters in the reanalysis record from 1960–2004, in three 50-year-long perpetual ENSO GEOSCCM integrations, and in models discussed in the CCMVal-2 report. A dashed line represents the average SSW frequency in the reanalysis record (cf. Table 1).

explanation presented in Section 3.1. We first show that the explanation presented in Section 3.1 is able to explain the intraensemble variability in EN and LN SSW frequency. Then, in Section 3.3, we will discuss each model individually.

[19] Consider first Figure 5a, where we plot the LN to EN ratio of extreme height anomalies in the SSW precursor region versus the ratio of fSSW. The correlation between the two is shown in the panel title. It is clear from the figure that the LN to EN ratio of extreme height anomalies in the

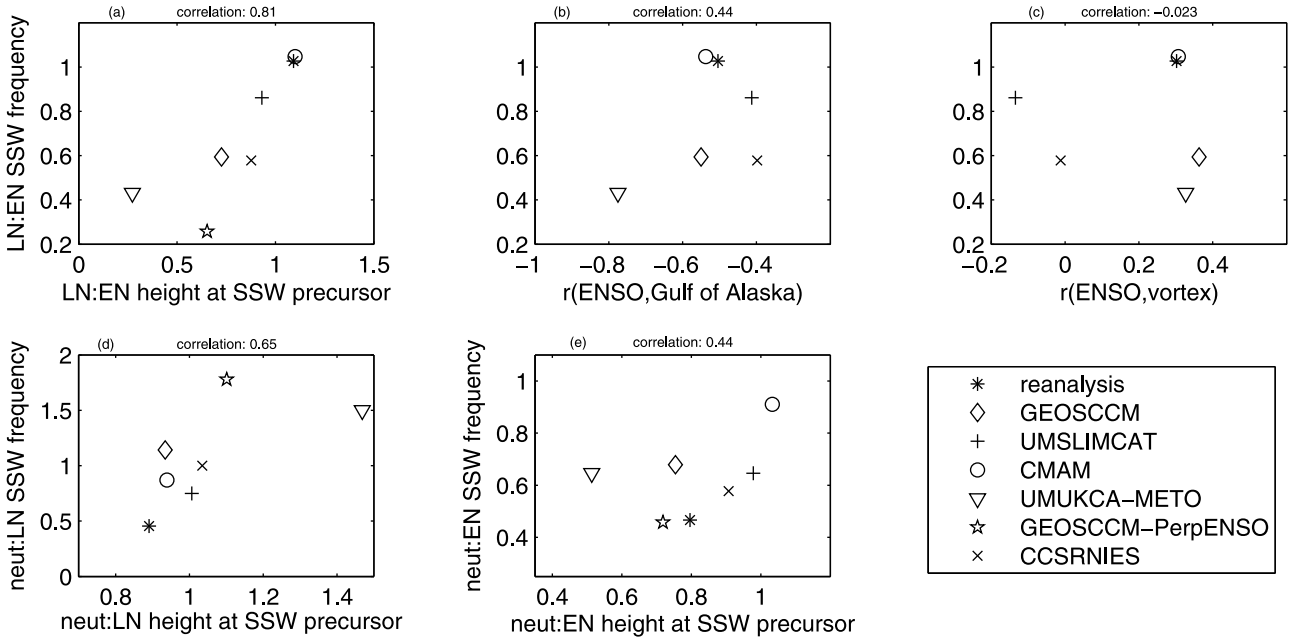

Figure 5. The relationship between LN and EN SSWs and the tropospheric and seasonal mean stratospheric effect of ENSO in NDJFM for each data source. Each marker represents one data source (i.e. reanalysis data or a model). (top)The relationship between the ratio of LN SSW frequency to EN SSW frequency and (a) the ratio of LN to EN extreme negative height anomalies in the SSW precursor region, (b) the correlation between the seasonal mean ENSO value and the seasonal mean Gulf of Alaska (35°N–55°N, 190°E–220°E) height anomaly, and (c) like Figure 5b but of ENSO with the seasonal mean polar vortex strength. (bottom) Like Figure 5a except for (d) the ratio of LN to neutral ENSO and (e) the ratio of EN to neutral ENSO. Note that diagnostics for the perpetual ENSO GEOSCCM experiment are only shown in Figures 5a, 5d, and 5e because of the nature of the experimental design.

tropospheric SSW precursor region is highly correlated with the LN to EN ratio of SSWs ($p > .98$). This strongly suggests that the inter-model variability in EN and LN fSSW is related to inter-model variability in the ability of ENSO teleconnections to penetrate the SSW precursor region. The explanation offered in Section 3.1 appears to explain the behavior in the other data sources as well.

[20] One might hypothesize that a model in which ENSO has a stronger impact on the Gulf of Alaska region might also have a larger difference between EN SSW and LN SSW frequency. To test this, we evaluate whether the strength of ENSO's teleconnection in the Gulf of Alaska region (defined in Section 2), rather than in the SSW precursor region, might be a better predictor of the ratio of LN to EN SSW frequency. Figure 5b shows the correlation of seasonal mean height anomalies in the Gulf of Alaska and the seasonal mean value of ENSO on the abscissa, and the ratio of LN to EN fSSW on the ordinate. The strength of ENSO teleconnections appears well correlated with the ratio of LN to EN fSSW (with $p > 0.8$). However, the inter-model variability in LN to EN fSSW is explained more closely by the frequency of extreme negative events in the SSW precursor region (i.e. Figure 5a). This clearly indicates that the frequency of extreme negative events in the SSW precursor region is more closely related to LN and EN fSSW than the impact of ENSO in the Gulf of Alaska.

[21] We next consider the relationship between the seasonal mean stratospheric response to ENSO and the effect of ENSO on SSWs. One might hypothesize that the seasonal mean stratospheric response to ENSO and the effect of ENSO on SSWs are closely related, and that a data set with a larger LN fSSW must necessarily have a weaker seasonal mean stratospheric vortex during LN. To demonstrate that this is not the case, Figure 5c compares the correlation between ENSO and the seasonal mean stratospheric vortex strength (defined in Section 2) to the ratio of LN to EN fSSW in each model. We find that the seasonal mean stratospheric response is not correlated with the ratio of LN to EN SSW frequency. Models that capture the seasonal mean stratospheric response to ENSO do not necessarily capture the correct LN to EN SSW frequency, and vice versa. The independence of the effect of ENSO on seasonal mean vortex strength from the effect of ENSO on SSW is consistent with the independence on interannual timescales found in BP11. In addition, *Charlton and Polvani* [2007] (see their see section 5a) find that at 10 hPa, the recovery from a SSW is sufficiently fast that the occurrence of a SSW has a weak effect on the seasonal mean vortex strength. They also find little relationship between seasonal mean wave driving of the vortex (which is modulated by ENSO) and the occurrence of a SSW. Finally, Figure 3 also demonstrates that the effect of ENSO on lower stratospheric heat flux differs between the seasonal mean and the intraseasonal extremes.

[22] BP11 also found that fSSW during neutral ENSO winters was lower than during either EN or LN winters. We test whether our explanation might be applicable to this effect as well. Figure 5d shows the relationship between extreme height anomalies in the SSW precursor region for each model during neutral ENSO and LN winters and the ratio of neutral ENSO to LN SSW frequency. The neutral ENSO to LN ratio of extreme height anomalies in the tropospheric SSW precursor region is highly correlated with the neutral ENSO to LN ratio of SSWs, though one model appears to be an outlier. This suggests that the inter-model variability in neutral ENSO fSSW is related to inter-model variability in the frequency of extreme anomalies in the SSW precursor region during neutral ENSO winters. Finally, Figure 5e is similar to Figure 5d, but shows the ratio of neutral ENSO to EN winters. Again, we find that the ratio of extreme height anomalies in the SSW precursor region is highly correlated with the ratio of SSW frequency, with the same model again an outlier. In summary, the intra-ensemble variability in the ratio of LN, neutral ENSO, and EN fSSW is closely linked to whether ENSO teleconnections result in extreme anomalies in the SSW precursor region.

3.3. Understanding SSW Frequency in Each Model

[23] In this section, we consider the LN and EN fSSW for each model in the context of the explanation we have presented. We will show that models that capture the processes highlighted above are able to capture the observed relationship between ENSO and SSW frequency. First, a model must realistically simulate the tropospheric teleconnections in the subpolar North Pacific in response to EN and LN. Second, a model must realistically simulate the tropospheric precursors of SSW events. If either of these processes is poorly simulated by a model, we find that that the resulting EN and/or LN fSSW does not match the observations.

[24] Figures 6 and 7 show the ENSO teleconnections and SSW precursors for the models in Table 1, with one model for each row in the figures. The SSW precursor anomalies are generally captured in the CCM integrations (Figure 6, right, and 7, right); the general agreement is indicated by the large pattern correlation with the reanalysis (in Figure 1c) shown on the right panel of each row and can be seen in the proximity of the diamond to the square. In addition, all models capture the gross features of EN and LN teleconnections, namely a trough and ridge respectively in the Gulf of Alaska near the star (though the magnitude certainly varies, as in *Cagnazzo et al.* [2009]). These gross similarities notwithstanding, subtle differences exist between the models, however: we now focus on these subtle differences and thereby shed light on the simulated fSSW during EN and LN in each model.

[25] 1. In the GEOSCCM perpetual-ENSO experiments (Figure 6, top), the modeled EN teleconnection and tropospheric precursors of SSWs are grossly similar to the observations. However, the modeled LN teleconnection is not true to observations in the Northwest Pacific (at the square on Figure 1b versus Figure 6b). Namely, the anomalous ridge generated by LN in the GEOSCCM model extends into the SSW precursor region in the subpolar Northwest Pacific. More importantly for SSWs, LN events lead to a statistically significant reduction in extreme negative height anomalies in the SSW precursor region (see the star in Figure 5a). It is therefore expected that fSSW in EN, but not in LN, is similar to that in the observations, as demonstrated in Figure 4b. Even though GEOSCCM captures ENSO teleconnections in the Gulf of Alaska, the teleconnections in the Northwest Pacific in LN, and hence the fSSW, do not resemble that in the reanalysis.

[26] 2. In the GEOSCCM CCMVal2 integration (Figure 6, middle row), the ENSO teleconnections are similar to,

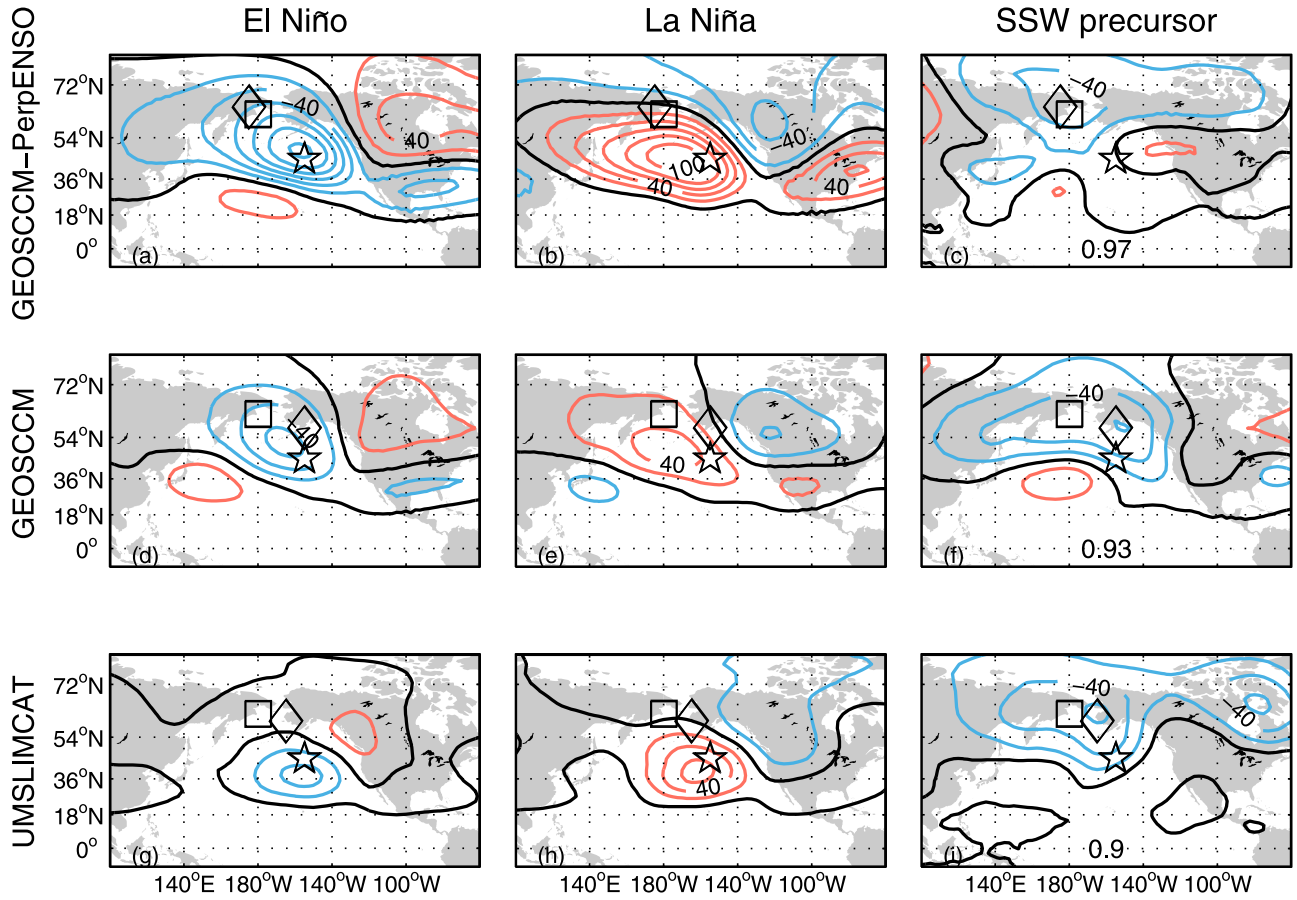

Figure 6. Like Figure 1 but for 3 CCMs. (a–c) For the perpetual El Niño and La Niña integrations as compared to the perpetual neutral ENSO integration (e.g., perp. EN-perp. ENSO neutral). (d–f) For the GEOSCCM CCMVal-2 integrations. (g–i) For the UMSLIMCAT. The contour interval is 10 m. Squares and stars are as in Figure 1, but diamonds represent the SSW precursor region for each model; see the text for details. The pattern correlation in the region 40N–75N, 165E–215E between the tropospheric precursors in the reanalysis and in each model is shown below each plot.

though weaker than, the ENSO teleconnections in the perpetual ENSO experiments. The tropospheric precursors of SSWs are also similar. The anomalous ridge generated by LN in the GEOSCCM model extends into the subpolar Northwest Pacific SSW precursor region. Because extreme negative anomalies in the SSW precursor region are suppressed, SSWs are suppressed during LN in the GEOSCCM CCMVal-2 integration as well (Figure 4c).

[27] 3. In UMSLIMCAT (Figure 6, bottom), the anomalous ridge generated by LN does not extend to the subpolar North Pacific, and the SSW precursors are captured realistically. Because the anomalous ridge generated by LN is meridionally confined (compared to, e.g., GEOSCCM), extreme negative height anomalies in the SSW precursor region occur with similar frequency during LN winters and EN winters (see the cross in Figure 5a). It is therefore to be expected that fSSW is similar in EN and LN (Figure 4d).

[28] 4. CMAM realistically captures SSW precursors (Figure 7c). Even though SSWs occur too frequently in CMAM (and therefore SSWs could conceivably be less sensitive to tropospheric variability), the characteristic tropospheric precursors of SSWs are present in CMAM. CMAM appears to capture the subpolar teleconnections of LN, though there is some intra-ensemble variability (not shown) and the anomalies are too weak. Most importantly for SSWs, however, the frequency of extreme negative height anomalies in the SSW precursor region is similar in all phases of ENSO (e.g., see the circle in Figures 5a and 5f). It is therefore to be expected that fSSW is similar in EN, neutral ENSO, and LN (Figure 4e).

[29] 5. SSW precursors in UMUKCA-METO (Figure 7f) do not resemble those in the reanalysis (the pattern correlation between Figure 7f and Figure 1c is lower for UMUKCA-METO than for any other model). Instead of an anomalous trough in the SSW precursor region, an anomalous trough is found in the Gulf of Alaska, near the center of the ridge associated with LN. The diamond is adjacent to the star and not to the square. The pattern correlation between Figures 7e and 7f in the region 40N–75N, 165E–215E is very low (−0.19). Consistent with this, extreme negative height anomalies occur less frequently in the SSW precursor region during LN winters and more frequently during EN winters (see the triangle in Figure 5a). It is therefore

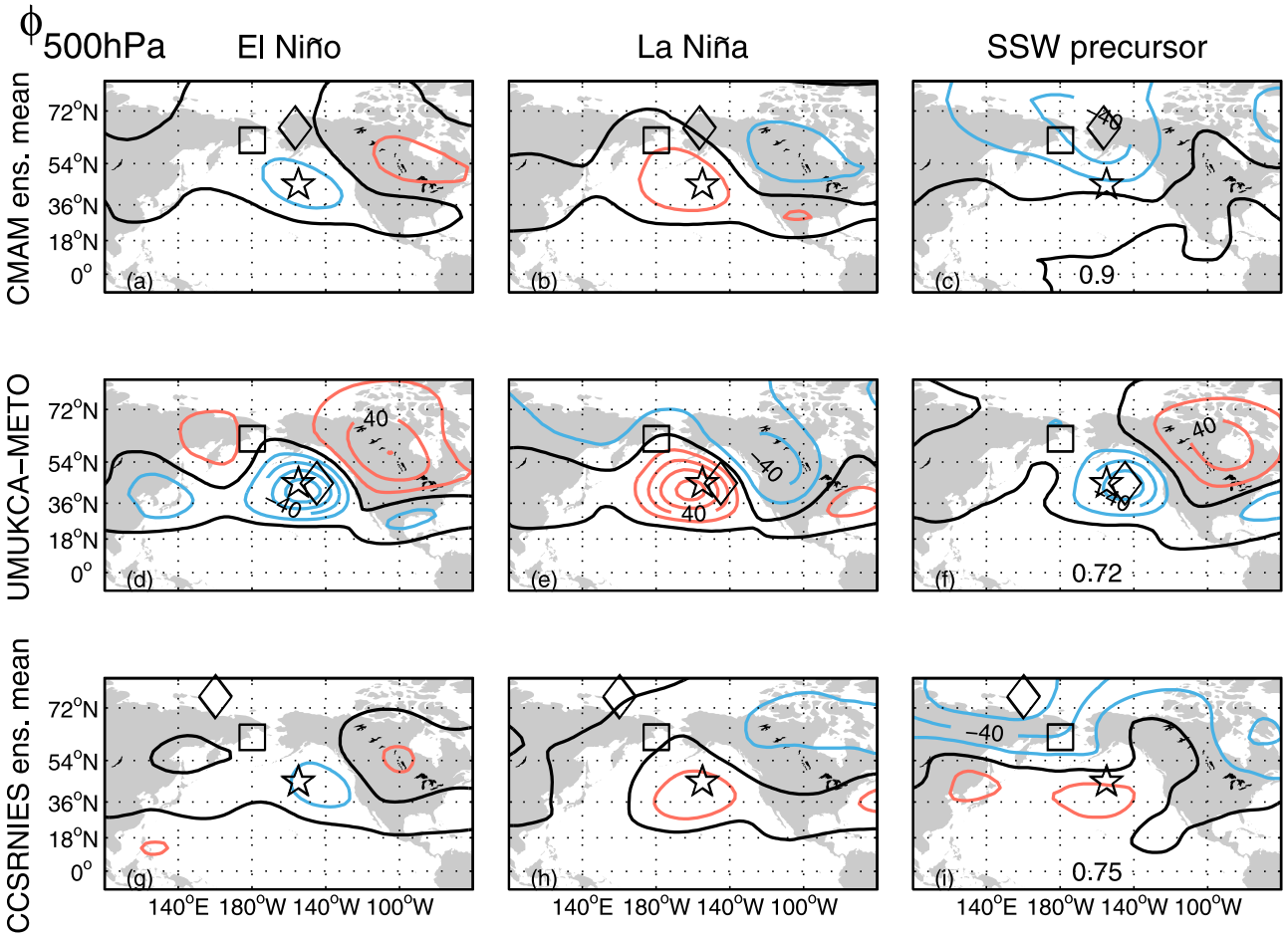

Figure 7. Like Figure 6 but for three other CCMVal-2 model integrations: (a–c) CMAM, (d–f) UMUKCA-METO, and (g–i) CCSRNIES.

expected that in UMUKCA-METO, LN suppresses SSWs (Figure 4f).

[30] 6. Finally, SSW precursors in CCSRNIES (Figure 7i) are displaced to the northwest of those in the reanalysis and are located outside of the region most strongly influenced by ENSO. In addition, ENSO teleconnections in this model are too weak. Neither process is captured well as compared to the reanalysis. Most importantly for SSWs, however, extreme negative height anomalies occur less frequently in the SSW precursor region during LN winters as compared to EN winters (see the "x" in Figure 5a), consistent with the decreased fSSW during LN (Figure 4g).

[31] In summary, models with realistic tropospheric teleconnections in the subpolar North Pacific during LN winters and realistic tropospheric precursors of SSWs have realistic fSSW in LN winters. This affirms the explanation offered in Section 3.1.

4. Conclusions

[32] Reanalysis data and chemistry-climate models are used to understand the connection between sudden stratospheric warmings and teleconnection patterns due to ENSO. The key point of this paper is that the region in the North Pacific most strongly associated with SSWs (the SSW precursor region) is distinct from the region most influenced by El Niño and La Niña. In the reanalysis, La Niña's canonical North Pacific ridge does not reach the subpolar Northwestern Pacific region that most strongly forces SSWs. Rather, we find that both El Niño and La Niña lead to more frequent extreme low anomalies in the SSW precursor region (cf. Figures 5a, 5d, and 5e). This explains why the frequency of SSWs is increased during both El Niño and La Niña winters.

[33] In the ensemble of models examined, the inter-model variability in La Niña and El Niño SSW frequency is found to be tightly correlated with the ability of ENSO teleconnections to penetrate the SSW precursor region. In addition, the ratio of SSW frequency during neutral ENSO and La Niña winters is tightly correlated with anomalies in the SSW precursor region. Many of the models here examined fail to capture this effect, and they therefore fail to realistically simulate El Niño and La Niña SSW frequency. For example, in two versions of the GEOS CCM, the ridge of La Niña's teleconnection extends beyond the Northwest Pacific to Eastern Russia, and so SSWs occur less frequently in La Niña winters than in El Niño winters. In addition, we confirm previous studies who have shown that the seasonal mean stratospheric vortex response to ENSO is not closely related to the effect of ENSO on SSWs.

[34] However, we acknowledge that we are unable to rule out the possibility that, for example, the GEOSCCM model is accurately simulating La Niña teleconnections and that the observed frequency of SSWs during La Niña winters is an artifact of the relatively short data record [note that the difference between LN and neutral ENSO fSSW is significant at the 90% level in the reanalysis record [*Butler and Polvani*, 2011]. Although *Hoskins and Karoly* [1981], *Sardeshmukh and Hoskins* [1988], and *Simmons et al.* [1983] provide a theory that can successfully explain the gross features of the wave train generated by anomalous ENSO convection, we are not aware of a theory that can explain the details of the subpolar Northwestern Pacific response to ENSO. Furthermore, different ensemble members of the same model can differ in the subpolar extent of ENSO teleconnections (not shown). It is therefore not entirely clear whether the "true" response to La Niña in the Northwestern Pacific more closely resembles the response in GEOSCCM or the response in the reanalysis (or in, e.g., UMSLIMCAT). For example, small changes in the strength or position of the climatological subtropical jet can lead to altered wave propagation (e.g., due to the QBO in *Garfinkel and Hartmann* [2010] or due to doubled CO_2 in *Meehl et al.* [2006]), and the GEOSCCM-climatological state in the North Pacific, like that in any model [e.g., *Ting and Sardeshmukh*, 1993], is not perfect. On the other hand, the observed relative frequencies of extreme negative height anomalies in the SSW precursor region in the different ENSO phases are not statistically distinct. Longer model integrations and more observational data are necessary before these results can be stated unequivocally. Nevertheless, the two processes identified in this study - the subpolar extent of La Niña teleconnections and tropospheric precursors of SSWs - will very likely be important pieces of the puzzle connecting ENSO and SSW events in the future.

Appendix A: Stratospheric Anomalies During SSWs in LN and EN

[35] One might ask whether the types of EN and LN SSWs are distinct and whether qualitatively different precursors are associated with SSWs in each ENSO phase [see, e.g., *Cohen and Jones*, 2011]. We therefore briefly document the type of the SSWs during LN and EN winters in the observational record. LN and EN SSWs prior to 2003 are evenly split between splitting events and displacement events [cf. *Charlton and Polvani*, 2007]. Specifically there were 5 split and 6 displacement during EN and 7 split and 4 displacement during LN in the ERA-40 reanalysis, and 5 split and 5 displacement during EN and 6 split and 5 displacement during LN in the NCAR/NCEP reanalysis [*Kalnay et al.*, 1996]. When we include the winters since 2002 (type taken from Table 1 of *Cohen and Jones* [2011]), we find a similar ratio of split versus displacement events during EN and LN. We have examined the tropospheric precursors for LN and EN SSWs, and while height anomalies in the troposphere bear a slight wave-2 signature during LN (not shown), the tropospheric precursors discussed in Section 3 dominate the LN SSWs as well. Finally, we note that differences in SSW type among the different phases of ENSO are not present in the long GEOSCCM perpetual ENSO experiments (not shown), even though the GEOSCCM is capable of capturing wave-1 and wave-2 patterns associated with SSWs [e.g., *Hurwitz et al.*, 2012]. While there might be subtle differences between the type of EN and LN SSW, these differences are not statistically robust and do not appear to be related to SSW frequency. Finally, *Garfinkel et al.* [2010] found that Northwest Pacific variability is important for wave driving associated with both wave-1 and wave-2. We therefore do not condition the SSW precursors based on the different SSW types.

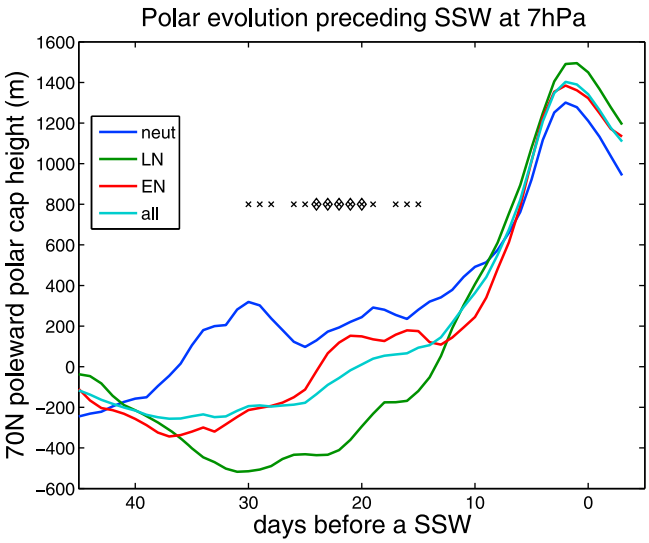

Figure A1. Anomalies of polar cap geopotential height at 7hpa leading up to a SSW for El Niño, La Niña, and Neutral ENSO only. Statistically significant differences at the 95% (90%) level between the El Niño and La Niña responses are indicated with diamonds (cross). Statistical significance is determine with a 2-tailed Student-T test.

[36] We now discuss the possible differences in the preconditioning of the vortex; that is, does the vortex strength a month before the SSWs differ between EN and LN SSWs? We find that the preconditioning of the vortex is roughly similar between LN winters and EN winters at 30–40 day lead times, though the vortex in LN is stronger at intermediate leads, however (Figure A1). In contrast, the preconditioning of neutral ENSO SSWs is dramatically (and significantly) different: the vortex begins weakening over a month before the central date. Neutral ENSO SSWs are also more likely to be displacement events (4 displacement versus 1 split); whether this difference can explain the different types for neutral ENSO SSWs, or is expected to persist in future neutral ENSO SSWs, is a topic for future work. We find that the seasonal mean vortex is strengthened by LN in all models examined in Sections 3.2–3.3 except for UMSLIMCAT (e.g., Figure 5c), yet UMSLIMCAT still has a high LN SSW frequency. Preconditioning of the vortex is therefore likely not the dominant cause for the enhanced LN SSW frequency. Finally, during all phases of ENSO, SSWs are of roughly similar strength (Figure A1).

[37] **Acknowledgments.** This work was supported by NASA grant NNX06AE70G and NSF grant ATM 0905863. The work of L.M.P. is funded, in part, by a grant of the US National Science Foundation to Columbia University. We thank Andrew Charlton-Perez for providing the SSW central dates for the CCMVal-2 models.

References

Akiyoshi, H., L. B. Zhou, Y. Yamashita, K. Sakamoto, M. Yoshiki, T. Nagashima, M. Takahashi, J. Kurokawa, M. Takigawa, and T. Imamura (2009), A CCM simulation of the breakup of the Antarctic polar vortex in the years 1980–2004 under the CCMVal scenarios, *J. Geophys. Res.*, *114*, D03103, doi:10.1029/2007JD009261.

Andrews, D. G., J. R. Holton, and C. B. Leovy (1987), *Middle Atmosphere Dynamics*, Academic, San Diego, Calif.

Baldwin, M. P., D. B. Stephenson, D. W. J. Thompson, T. J. Dunkerton, A. J. Charlton, and A. O'Neill (2003), Stratospheric memory and skill of extended-range weather forecasts, *Science*, *301*, 636–640, doi:10.1126/science.1087143.

Bell, C. J., L. J. Gray, A. J. Charlton-Perez, M. M. Joshi, and A. A. Scaife (2009), Stratospheric communication of El Niño teleconnections to European winter, *J. Clim.*, *22*, 4083–4096, doi:10.1175/2009JCLI2717.1.

Brönnimann, S. (2007), Impact of El Niño–Southern Oscillation on European climate, *Rev. Geophys.*, *45*, RG3003, doi:10.1029/2006RG000199.

Butler, A. H., and L. M. Polvani (2011), El Niño, La Niña, and stratospheric sudden warmings: A reevaluation in light of the observational record, *Geophys. Res. Lett.*, *38*, L13807, doi:10.1029/2011GL048084.

Cagnazzo, C., et al. (2009), Northern winter stratospheric temperature and ozone responses to ENSO inferred from an ensemble of chemistry climate models, *Atmos. Chem. Phys. Discuss.*, *91*, 12,141–12,170.

Charlton, A. J., and L. M. Polvani (2007), A new look at stratospheric sudden warmings. Part I: Climatology and modeling benchmarks, *J. Clim.*, *20*, 449–469, doi:10.1175/JCLI3996.1.

Cohen, J., and J. Jones (2011), Tropospheric precursors and stratospheric warmings, *J. Clim.*, *24*, 6562–6572, doi:10.1175/2011JCLI4160.1.

Dunkerton, T. J., C. P. Hsu, and M. E. McIntyre (1981), Some Eulerian and Lagrangian diagnostics for a model stratospheric warming, *J. Atmos. Sci.*, *38*, 819–843, doi:10.1175/1520-0469.

Eyring, V., M. P. Chipperfield, M. A. Giorgetta, D. E. Kinnison, E. Manzini, K. Matthes, P. A. Newman, S. Pawson, T. G. Shepherd, and D. W. Waugh (2008), Overview of the new CCMVal reference and sensitivity simulations in support of upcoming ozone and climate assessments and the planned SPARC CCMVal report, *SPARC Newsl.*, *30*, 20–26.

Free, M., and D. J. Seidel (2009), Observed El Niño–Southern Oscillation temperature signal in the stratosphere, *J. Geophys. Res.*, *114*, D23108, doi:10.1029/2009JD012420.

Garfinkel, C. I., and D. L. Hartmann (2007), Effects of the El Niño–Southern Oscillation and the Quasi-Biennial Oscillation on polar temperatures in the stratosphere, *J. Geophys. Res.*, *112*, D19112, doi:10.1029/2007JD008481.

Garfinkel, C. I., and D. L. Hartmann (2008), Different ENSO teleconnections and their effects on the stratospheric polar vortex, *J. Geophys. Res.*, *113*, D18114, doi:10.1029/2008JD009920.

Garfinkel, C. I., and D. L. Hartmann (2010), The influence of the quasi-biennial oscillation on the North Pacific and El Niño teleconnections, *J. Geophys. Res.*, *115*, D20116, doi:10.1029/2010JD014181.

Garfinkel, C. I., D. L. Hartmann, and F. Sassi (2010), Tropospheric precursors of anomalous Northern Hemisphere stratospheric polar vortices, *J. Clim.*, *23*, 3282–3299.

Garfinkel, C. I., S. Feldstein, D. W. Waugh, C. Yoo, and S. Lee (2012), Observed connection between stratospheric sudden warmings and the Madden-Julian Oscillation, *Geophys. Res. Lett.*, doi:10.1029/2012GL053144, in press.

Hoerling, M. P., A. Kumar, and M. Zhong (1997), El Niño, La Niña, and the nonlinearity of their teleconnections, *J. Clim.*, *10*, 1769–1786.

Horel, J. D., and J. M. Wallace (1981), Planetary scale atmospheric phenomena associated with the Southern Oscillation, *Mon. Weather Rev.*, *109*, 813–829.

Hoskins, B. J., and D. Karoly (1981), The steady linear response of a spherical atmosphere to thermal and orographic forcing, *J. Atmos. Sci.*, *38*, 1179–1196.

Hurwitz, M. M., P. A. Newman, F. Li, L. D. Oman, O. Morgenstern, P. Braesicke, and J. A. Pyle (2010), Assessment of the breakup of the Antarctic polar vortex in two new chemistry-climate models, *J. Geophys. Res.*, *115*, D07105, doi:10.1029/2009JD012788.

Hurwitz, M. M., I.-S. Song, L. D. Oman, P. A. Newman, A. M. Molod, S. M. Frith, and J. E. Nielsen (2011), Response of the Antarctic stratosphere to warm pool El Niño events in the GEOS CCM, *Atmos. Chem. Phys.*, *11*, 9659–9669, doi:10.5194/acp-11-9659-2011.

Hurwitz, M. M., P. A. Newman, and C. I. Garfinkel (2012), On the influence of North Pacific sea surface temperature on the Arctic winter climate, *J. Geophys. Res.*, doi:10.1029/2012JD017819, in press.

Ineson, S., and A. A. Scaife (2009), The role of the stratosphere in the European climate response to El Niño, *Nat. Geosci.*, *2*, 32–36, doi:10.1038/ngeo381.

Kalnay, E., et al. (1996), The NCEP/NCAR 40-Year Reanalysis Project, *Bull. Am. Meteorol. Soc.*, *77*, 437–472, doi:10.1175/1520-0477(1996)077<0437:TNYRP>2.0.CO;2.

Limpasuvan, V., D. W. J. Thompson, and D. L. Hartmann (2004), The life cycle of the Northern Hemisphere sudden stratospheric warmings, *J. Clim.*, *17*, 2584–2596.

Limpasuvan, V., D. L. Hartmann, D. W. J. Thompson, K. Jeev, and Y. L. Yung (2005), Stratosphere-troposphere evolution during polar vortex intensification, *J. Geophys. Res.*, *110*, D24101, doi:10.1029/2005JD006302.

Manzini, E., M. A. Giorgetta, L. Kornbluth, and E. Roeckner (2006), The influence of sea surface temperatures on the northern winter stratosphere: Ensemble simulations with the MAECHAM5 model, *J. Clim.*, *19*, 3863–3881.

Matsuno, T. (1971), A dynamical model of the stratospheric sudden warming, *J. Atmos. Sci.*, *28*, 1479–1494.

Meehl, G. A., H. Teng, and G. Branstator (2006), Future changes of El Niño in two global coupled climate models, *Clim. Dyn.*, *26*, 549–566, doi:10.1007/s00382-005-0098-0.

Mitchell, D. M., L. J. Gray, and A. J. Charlton-Perez (2011), The structure and evolution of the stratospheric vortex in response to natural forcings, *J. Geophys. Res.*, *116*, D15110, doi:10.1029/2011JD015788.

Morgenstern, O., P. Braesicke, F. M. O'Connor, A. C. Bushell, C. E. Johnson, S. M. Osprey, and J. A. Pyle (2009), Evaluation of the new UKCA climate-composition model - Part 1: The stratosphere, *Geosci. Model Dev.*, *2*, 43–57.

Nishii, K., H. Nakamura, and T. Miyasaka (2009), Modulations in the planetary wave field induced by upward-propagating rossby wave packets prior to stratospheric sudden warming events: A case-study, *Q. J. R. Meteorol. Soc.*, *135*(638), 39–52, doi:10.1002/qj.359.

Nishii, K., H. Nakamura, and Y. J. Orsolini (2010), Cooling of the wintertime Arctic stratosphere induced by the western Pacific teleconnection pattern, *Geophys. Res. Lett.*, *37*, L13805, doi:10.1029/2010GL043551.

Polvani, L. M., and D. W. Waugh (2004), Upward wave activity flux as a precursor to extreme stratospheric events and subsequent anomalous surface weather regimes, *J. Clim.*, *17*, 3548–3554.

Rienecker, M. M., et al. (2008), The GEOS-5 Data Assimilation System—Documentation of versions 5.0.1, 5.1.0, and 5.2.0, *NASA Tech. Memo.*, *NASA TM/2008-104606*, vol. 27, 118 pp.

Rienecker, M. M., et al. (2011), MERRA: NASA's Modern-Era Retrospective Analysis for Research and Applications, *J. Clim.*, *24*, 3624–3648, doi:10.1175/JCLI-D-11-00015.1.

Sardeshmukh, P. D., and B. J. Hoskins (1988), The generation of global rotational flow by steady idealized tropical divergence, *J. Atmos. Sci.*, *45*, 1228–1251.

Sassi, F., D. Kinnison, B. A. Bolville, R. R. Garcia, and R. Roble (2004), Effect of El-Niño–Southern Oscillation on the dynamical, thermal, and chemical structure of the middle atmosphere, *J. Geophys. Res.*, *109*, D17108, doi:10.1029/2003JD004434.

Scinocca, J. F., N. A. McFarlane, M. Lazare, J. Li, and D. Plummer (2008), Technical Note: The CCCma third generation AGCM and its extension into the middle atmosphere, *Atmos. Chem. Phys.*, *8*, 7055–7074.

Simmons, A., J. M. Wallace, and G. Branstator (1983), Barotropic wave propagation and instability, and atmospheric teleconnection patterns, *J. Atmos. Sci.*, *40*, 1363–1392.

SPARC CCMVal (2010), SPARC report on the evaluation of chemistry-climate models, *SPARC Rep. 5*, Univ. of Toronto, Toronto, Ont., Canada. [Available at http://www.atmosp.physics.utoronto.ca/SPARC.]

Taguchi, M., and D. L. Hartmann (2006), Increased occurrence of stratospheric sudden warming during El Niño as simulated by WAACM, *J. Clim.*, *19*, 324–332, doi:10.1175/JCLI3655.1.

Tian, W., and M. P. Chipperfield (2005), A new coupled chemistry-climate model for the stratosphere: The importance of coupling for future O_3-climate predictions, *Q. J. R. Meteorol. Soc.*, *131*, 281–303, doi:10.1256/qj.04.05.

Ting, M., and P. D. Sardeshmukh (1993), Factors determining the extratropical response to equatorial diabatic heating anomalies, *J. Atmos. Sci.*, *50*, 907–918.

Uppala, S. M., et al. (2005), The ERA-40 reanalysis, *Q. J. R. Meteorol. Soc.*, *77*(3), 437–471.

Woollings, T., A. Charlton-Perez, S. Ineson, A. G. Marshall, and G. Masato (2010), Associations between stratospheric variability and tropospheric blocking, *J. Geophys. Res.*, *115*, D06108, doi:10.1029/2009JD012742.